The human thalamus orchestrates neocortical oscillations during NREM sleep.

Thomas Schreiner[1], Elisabeth Kaufmann[2], Soheyl Noachtar[2], Jan-Hinnerk Mehrkens[3] & Tobias Staudigl[1]

1 Department of Psychology, Ludwig-Maximilians-Universität München, Munich, Germany

2 Epilepsy Center, Department of Neurology, Ludwig-Maximilians-Universität München, Munich, Germany

3 Department of Neurosurgery, Ludwig-Maximilians-Universität München, Munich, Germany

Correspondence: Tobias Staudigl (tobias.staudigl@lmu.de)

ABSTRACT

A hallmark of non-rapid eye movement (NREM) sleep is the coordinated interplay of slow oscillations (SOs) and sleep spindles. Traditionally, a cortico-thalamo-cortical loop is suggested to coordinate these rhythms: neocortically-generated SOs trigger spindles in the thalamus that are projected back to neocortex. Here, we used direct intrathalamic recordings from human epilepsy patients to test this canonical interplay. We show that SOs in the anterior thalamus precede neocortical SOs, whereas concurrently-recorded SOs in the mediodorsal thalamus are led by neocortical SOs. Furthermore, sleep spindles, detected in both thalamic nuclei, preceded their neocortical counterparts and were initiated during early phases of thalamic SOs. Our findings indicate an active role of the anterior thalamus in organizing the cardinal sleep rhythms in the neocortex and highlight the functional diversity of specific thalamic nuclei in humans. The concurrent coordination of sleep oscillations by the thalamus could have broad implications for the mechanisms underlying memory consolidation.

INTRODUCTION

The presence and coordinated interplay of slow oscillations (SOs) and sleep spindles hallmarks non-rapid eye movement (NREM) sleep [1–3]. SOs (~1 Hz) reflect neuronal network alterations of the membrane potential between periods of neuronal silence ('hyperpolarization', i.e., down state) and neuronal excitation (depolarization, i.e., up state) [4,5]. The origin of SOs has been traditionally located to neocortical circuits [5,6], triggering time windows of excitability and inhibition not only in neocortex but also in the thalamus and the hippocampus [5]. However, recent evidence from animal models casts doubt on the view that SOs are exclusively initiated and orchestrated by neocortical activity and suggest that the thalamus plays a critical role in synchronizing and coordinating SO activity [7–12].

The depolarizing phase of SOs is assumed to initiate the generation of sleep spindles within the thalamic circuitry [13]: reciprocal interactions between the thalamic reticular nucleus and thalamocortical neurons result in waxing and waning oscillations in the range of 11-16 Hz. Sleep spindles are usually nested towards the excitable up states of neocortical SOs [14–16], and are also found in the hippocampus, where they are thought to synchronize hippocampal ripples [17–19].

Importantly, this triple-coupling of sleep related oscillations has been suggested to facilitate memory consolidation, by synchronizing neuronal activity across brain regions and relaying memory representations between the hippocampus and neocortical long-term stores [20,21]. While a plethora of studies bolster the critical role of sleep oscillations and their coordinated interplay for the memory function of sleep [3,22], the exact neural circuits enabling their complex orchestration across brain areas are less clear, ultimately impeding our understanding of the prime mechanistic vehicle of memory consolidation.

This is particularly striking with respect to the neural circuits facilitating memory consolidation in humans, since direct neural recordings from one of the key players, the thalamus, are scarce. The anterior thalamic nuclei (ANT) and the mediodorsal thalamus (MD) have recently taken center-stage as thalamic key areas for different aspects of human memory functions [23,24], and might therefore also play a key role in coordinating sleep oscillations relevant for memory consolidation. Leveraging the rare opportunity to record intracranial electroencephalography (iEEG) from the human ANT and MD, together with simultaneous scalp electroencephalography (EEG), we investigated the interplay of NREM sleep oscillations within a thalamocortical network that is known to serve memory functions during wake[25].

We show that SOs in the ANT, but not the MD, lead neocortical SOs. These results undermine the notion of an exclusive generation of SOs in the human neocortex and highlight the functional diversity of specific thalamic nuclei. Sleep spindles in both the ANT and MD preceded neocortical spindles, in line with their thalamic origin[26]. Furthermore, we show that the nesting of sleep oscillations in the thalamus differs from the nesting in neocortex. Thalamic spindles locked to earlier thalamic SO-phases than their neocortical counterparts.

RESULTS

To examine thalamo-cortical interactions during human NREM sleep, we analyzed simultaneously-recorded intracranial thalamic and scalp EEG collected across 11 full nights of sleep from 8 patients with pharmaco-resistant epilepsy. On average, participants slept for 8.82 ± 1.41 hours, with 63.51 ± 0.07 % spent in NREM sleep (stages N2 and N3; see Supplementary Table 1 for proportions of times spent in each stage, Fig. 1c). Thalamic activity was recorded from the ANT and the MD (see Fig. 1a and methods for details on electrode localization). We isolated sleep oscillations from 27 bipolar intracranial thalamic channels (12 ANT; 15 MD) and scalp EEG electrodes (see Supplementary Table 2 for details).To determine thalamo-cortical coordination during NREM sleep and their specificity, we detected SOs, spindles and SO-spindle events independently in thalamic iEEG (ANT & MD) and scalp EEG recordings, assessed their coupling and delineated the temporal relationship of thalamo-cortical interactions (for descriptive values and characteristics see Supplementary Tables 3-6; Fig. 1b).

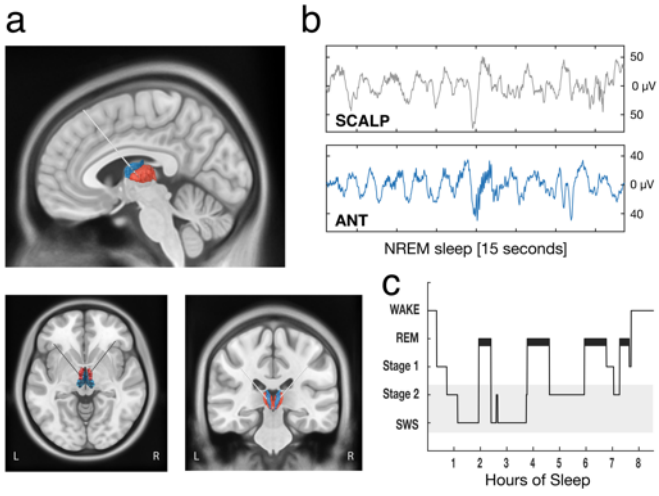

Fig 1. | Thalamic electrode placement and sleep architecture. **(a)** Electrodes were implanted in the left and right ANT (blue) and MD (red). **(b)** Example of NREM sleep segment (15 sec), comprising SOs and sleep spindles (top row: scalp recording; bottom row: ANT). **(c)** Hypnogram of a sample participant, showing time spent in different sleep stages across one recording night.

ANT SOs precede neocortical SOs

ANT SOs significantly preceded neocortical SOs, as revealed by occurrence probabilities of ANT SOs relative to neocortical SOs (Fig. 2a, significant positive cluster from -0.15 to 0.05 s, $p < 0.005$; tested against event-free occurrence probabilities; corrected for multiple comparisons across time). ANT SO occurrence preferentially peaked, on average, briefly before the emergence of neocortical SOs (time of peak: -0.05 sec). To further validate this outcome, we specifically determined the phase of ANT SOs for all paired SO-events (i.e., all ANT SOs within ± 750 ms of neocortical SOs) at the time of neocortical SO down state (i.e., thalamo-cortical SO phase-phase coupling). We found significant nonuniform distributions in each of the ANT contacts (12/12) ($p < 0.05$, corrected for multiple comparisons using the False Discovery Rate (FDR) [30]; Rayleigh test, mean vector length: 0.46 ± 0.05). Moreover, we found a significant nonuniform distribution across contacts (Rayleigh $z = 10.95$, $p < 0.0001$), with the phase of ANT SOs being ahead of their neocortical counterparts (the phase of neocortical SO down states corresponds to ± π; mean coupling direction: −176.39 ± 4.94°; see Fig. 2b).

To showcase the generic features of ANT and neocortical detected SOs, time-frequency representations (TFRs) of SO-locked neocortical (Fig. 2c) and ANT (Fig. 2e) activity were contrasted against event-free events. TFRs time-locked to scalp-derived SO down states exhibited the prototypical modulation of low frequency (< 5 Hz) and spindle power (11–16 Hz) during SO events (Fig. 2c). In particular, low frequency power peaked before the SO down state. In contrast, spindle power was diminished during the down state, increased during the positive deflections of the SO and peaked during the SO up state (significant clusters: $p < 0.05$, corrected for multiple comparisons across time and frequency). Remarkably, while low frequency power for ANT derived SOs showed similar pre-down state increases, power in the spindle band (11-16 Hz) and beyond (> 20 Hz) showed an early power increase tightly locked to the ANT SO down state (Fig. 2e; $p < 0.05$, corrected for multiple comparisons across time and frequency). This pattern deviates from generic modulations of spindles by SOs as described in our and previous scalp EEG recordings, where spindles nest towards SO up states [1,16]. Figure 2d illustrates the scalp EEG grand average, locked to the minimum of neocortical SO down states. Figure 2f illustrates the ANT grand average locked to the minimum of ANT SO down states.

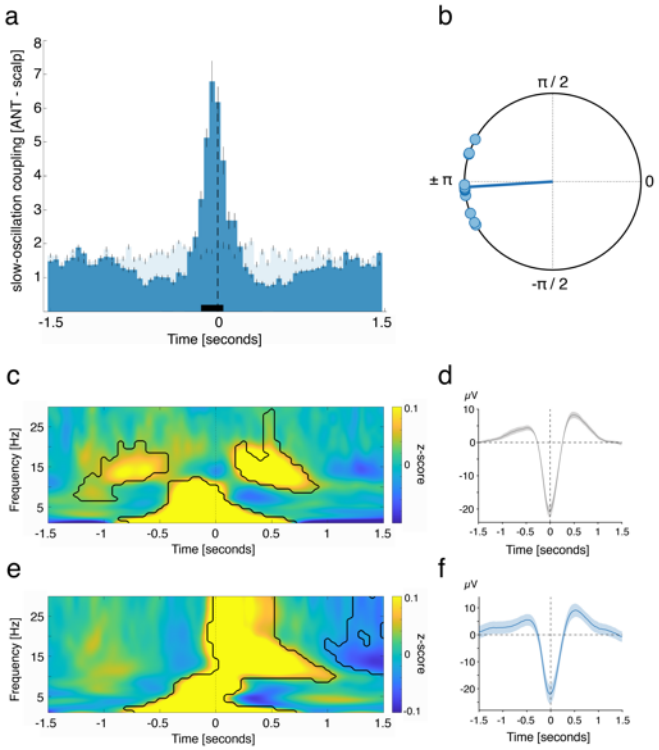

Fig 2. | ANT SOs precede neocortical SOs. (a) Occurrence probabilities of ANT SO down state peaks relative to neocortical SO down state peaks (time = 0; dashed line), indicating that ANT SOs precede neocortical SOs. The solid black bar indicates significant time bins, resulting from comparison with SO-free control events (significant positive cluster from -0.15 to 0.05 sec, $p < 0.005$; time of peak: -0.05 sec). (b) Phase of ANT SOs at the time of neocortical SO downstate for paired SO-SO events, illustrating that ANT SO phases preceded their neocortical counterparts (phase of neocortical SO down states corresponds to ± π; mean coupling direction: –176.39 ± 4.94°; Rayleigh test: $p < 0.0001$; $z = 10.95$). (c) Time–frequency representation of neocortical SOs (locked to neocortical SO down states), contrasted against event-free segments. The contour lines indicate significant clusters ($p < 0.05$, corrected for multiple comparisons across time and frequency). (d) Grand average EEG trace of neocortical SOs (mean ± SEM, negative peak, time 0). (e) Time–frequency representation of all ANT SOs (locked to ANT SO down states), contrasted against event-free segments. The contour lines indicate significant clusters ($p < 0.05$, corrected for multiple comparisons across time and frequency). (f) Grand average iEEG trace of ANT SOs (mean ± SEM, negative peak, time 0).

Neocortical SOs precede SOs in the MD

Next, we asked, whether SOs leading neocortical SOs is specific to the ANT or can also be found in other thalamic nuclei. To address this question, we investigated the interplay between neocortical SOs and SOs in the mediodorsal thalamus (MD).

In stark contrast to ANT SOs, SOs in the MD did not precede, but were on average led by neocortical SOs, as evidenced by occurrence probabilities (Fig. 3a; significant positive cluster from -0.05 to 0.1 s, $p = 0.021$; corrected for multiple comparisons across time; time of peak: 0.05 sec). Again, we determined the phase of thalamic SOs for all paired SO-events at the time of neocortical SO down state (± 750 ms). We found significant nonuniform distributions in all MD contacts (15/15, $p < 0.05$, corrected for multiple comparisons using FDR; Rayleigh test, mean vector length: 0.41 ± 0.06) and a significant nonuniform distribution across contacts (Rayleigh $z = 7.94$, $p = 0.0001$), with the phase

of MD SOs following their neocortical counterparts (mean coupling direction: 133.51 ± 10.91°; see Fig. 3b). TFRs time-locked to scalp-derived SO down states exhibited the typical modulation of low frequency (< 5 Hz) and spindle power (11–16 Hz) during SO events (Fig. 3c; $p < 0.05$, corrected for multiple comparisons across time and frequency). Similar to the ANT, TFRs locked to the down states of MD SOs exhibited significant low frequency power increases before the down state-peak (Fig. 3e, time = 0), and power increases in the sleep spindle band and beyond locked to the down state (significant cluster: $p < 0.05$, corrected for multiple comparisons across time and frequency). Figure 3d illustrates the scalp EEG grand average, locked to the minimum of neocortical SO down states. Figure 3f illustrates the MD grand average locked to the minimum of MD SO down states.

Finally, we directly compared ANT-neocortical and MD-neocortical interactions with regards to SOs and tested whether ANT SOs would systematically emerge earlier (in relation to neocortical SOs) than MD SOs. The occurrence probabilities of ANT SOs relative to neocortical SOs differed significantly from those obtained from MD SOs relative to neocortical SOs, with ANT SOs preferentially emerging before MD SOs (Fig 3g; significant positive cluster from -0.25 to -0.05 s, $p = 0.018$; corrected for multiple comparisons across time; for a direct comparison of ANT-MD SOs see Supplementary Fig. 1). Also, the phase distribution for the preferential coupling between thalamus and neocortex differed significantly when comparing ANT and MD related SO coupling (Fig. 3h; Watson-Williams test: $F = 12.7$, $p = 0.0015$), supporting the leading role of ANT SOs as compared to the MD.

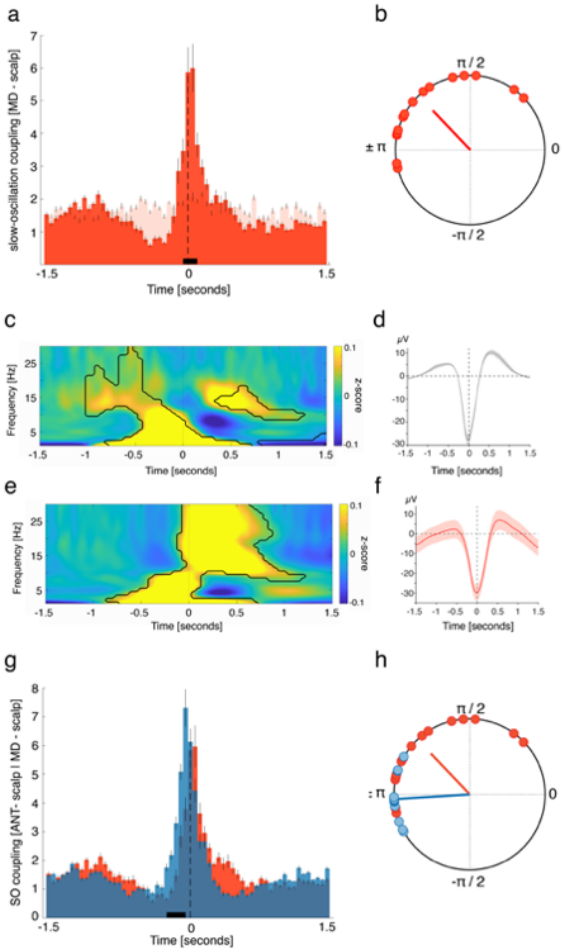

Fig 3. | Neocortical SOs precede SOs in the MD. (a) Occurrence probabilities of MD SO down state peaks relative to neocortical SO down state peaks (time = 0, dashed line), illustrating that, on average, neocortical SOs lead MD SOs. The solid black line indicates significant time bins, resulting from comparison with SO-free control events (significant positive cluster from -0.05 to 0.1 sec, p = 0.021; time of peak: 0.05 sec). (b) Phase of MD SOs at the time of neocortical SO downstate for paired SO-SO events, depicting that MD SO phases followed their neocortical counterparts (phase of neocortical SO down states corresponds to ± π; mean coupling direction: 133.51 ± 10.91°; Rayleigh test: $p < 0.0001$; $z = 7.94$). (c) Time–frequency representation of neocortical SOs (locked to neocortical SO down states), contrasted against event-free segments. The contour lines indicate significant clusters ($p < 0.05$, corrected for multiple comparisons across time and frequency). (d) Grand average EEG trace of neocortical SOs (mean ± SEM, negative peak, time 0). (e) Time–frequency representation of all MD SOs (locked to MD SO down states), contrasted against event-free segments. The contour lines indicate significant clusters ($p < 0.05$, corrected for multiple comparisons across time and frequency). (f) Grand average iEEG trace of MD SOs (mean ± SEM, negative peak, time 0). (g) Occurrence probabilities for the direct comparison of ANT-neocortical and MD-neocortical SO interactions, showing that ANT SOs preferentially emerge before MD SOs with regards to their neocortical counterparts (significant positive cluster from -0.25 to -0.05 sec, p = 0.018; corrected for multiple comparisons across time;). (h) The phase distribution for the coupling between thalamus and neocortex differed significantly when comparing ANT and MD related SO coupling (Watson-Williams test: $F = 12.7$, $p = 0.0015$).

ANT spindles precede neocortical spindles

Animal models established that sleep spindles are generated in the thalamus and spread to the neocortex along thalamocortical fibers [26]. However, it is unclear which of the many thalamic nuclei contribute to the generation of spindles and whether this translates to humans. Here, we show that the human ANT is putatively part of the spindle generating thalamic circuit, as ANT spindle occurrence peaked on average before the emergence of neocortical spindles (Fig. 4a; significant positive clusters: -2.5 to -0.05 s, $p < 0.005$ & 0.15 to 0.2 s, $p = 0.019$; corrected for multiple comparisons across time; time of peak: -0.1 sec).

We further assessed the interplay of ANT and neocortical sleep spindles using a complementary analytical approach. Specifically, we tested to what extend spindle-related oscillatory power-modulations would precede those in the neocortex, by computing power-power correlations in the sleep spindle band (see methods for details). We found a significant, off-diagonal cluster of temporal cross-correlations with regards to spindle power between ANT and neocortical sites ($p = 0.004$, cluster corrected across time; Fig. 4b), supporting our initial finding that ANT spindles lead their neocortical counterparts. Figure 4c and e depict the spindle-locked (time 0 = maximally negative amplitude) neocortical (Fig. 4c) and ANT (Fig. 4e) related TFRs. While the power of scalp derived spindles was confined to the classical sleep spindle range (~11-16 Hz; Fig. 4c), power increases in the spindle band transitioned seamlessly into higher frequencies (> 20 Hz) in case of ANT recordings (Fig. 4e; $p < 0.05$, corrected for multiple comparisons across time and frequency). Figure 4d and f illustrate the grand average electrophysiological traces across scalp electrodes / ANT contacts (mean ± SEM, respectively), locked to the neocortical (Fig. 4d) and ANT (Fig. 4f) sleep spindle peak (maximally negative amplitude, time 0). Figure 4d illustrates the scalp EEG grand average, locked to the neocortical sleep spindle peak. Figure 4f illustrates the ANT grand average, locked to the ANT sleep spindle peak.

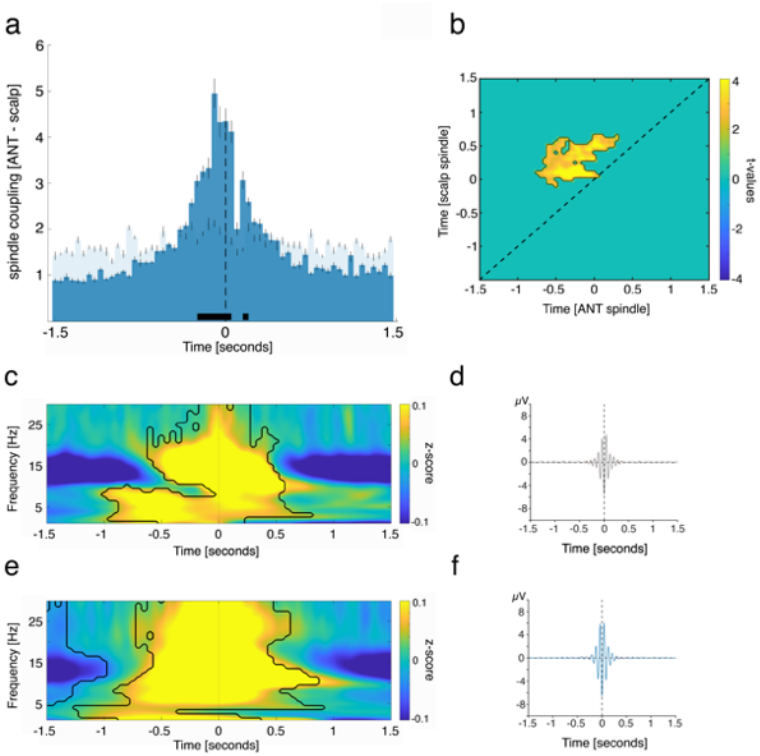

Fig 4. | **ANT spindles lead neocortical spindles.** **(a)** Occurrence probabilities of ANT spindle peaks relative to neocortical spindle peaks (maximal negative amplitude, time = 0; dashed line), indicating that ANT spindles precede neocortical spindles. The solid black line indicates significant time bins, resulting from comparison with spindle-free control events (significant positive clusters from -0.25 to -0.05 sec, $p < 0.005$ & 0.15 to 0.2 sec, $p = 0.019$; corrected for multiple comparisons across time; time of peak: -0.1 sec). **(b)** Power-power correlations in the sleep spindle band for paired spindle events (locked to neocortical spindle peak), contrasted against event-free correlation maps. The contour lines indicate the significant cluster ($p = 0.004$, cluster corrected across time), depicting that ANT related spindle power precedes neocortical spindle power. **(c)** Time–frequency representation of neocortical spindles (locked to neocortical spindle peak), contrasted against event-free segments. The contour lines indicate significant clusters ($p < 0.05$, corrected for multiple comparisons across time and frequency). **(d)** Grand average EEG trace of neocortical spindles (mean ± SEM, maximally negative amplitude, time 0). **(e)** Time–frequency representation of all ANT spindles (locked to ANT spindle peak), contrasted against event-free segments. The contour lines indicate significant clusters ($p < 0.05$, corrected for multiple comparisons across time and frequency). **(f)** Grand average iEEG trace of ANT spindles (mean ± SEM, maximally negative amplitude, time 0).

MD spindles lead neocortical spindles

Next, we tested the temporal relationship between MD and neocortical spindles. MD spindles occurred on average before neocortical spindles (Fig. 5a; significant positive clusters: -0.3 to 0.05 s, $p < 0.005$; corrected for multiple comparisons across time; time of peak: -0.05 sec). We also assessed power-power correlations in the sleep spindle band for neocortical- MD paired spindle events (locked to neocortical spindle peaks). We found a significant, off-diagonal cluster of temporal cross-correlation with regards to spindle power between MD and neocortical sites (Fig. 5b; tested against event-free segments; $p = 0.002$, cluster corrected across time), indicating that MD spindle-related power modulations preceded neocortical spindle-related power.

Fig. 5c and e depict the spindle-locked (maximally negative amplitude) neocortical and MD related TFRs. Power of scalp derived spindles was, as expected, confined to the classical sleep spindle range (~11-16 Hz; Fig. 5c), while TFRs related to MD spindles exhibited power increases in the spindle band and beyond (> 20 Hz). Overall, the relationship between MD spindles and neocortical spindles was highly similar to the relationship between ANT spindles and neocortical spindles (see Figs. 4a + b). Figure 5d illustrates the scalp EEG grand average, locked to the neocortical sleep spindle peak. Figure 5f illustrates the MD grand average, locked to the MD sleep spindle peak. Figure 5g shows a comparison of ANT-neocortical and MD-neocortical interactions with regards to spindles. The timing of ANT and MD-related spindles in relation to neocortical spindles was highly similar. No significant differences emerged (cluster with lowest $p = 0.52$).

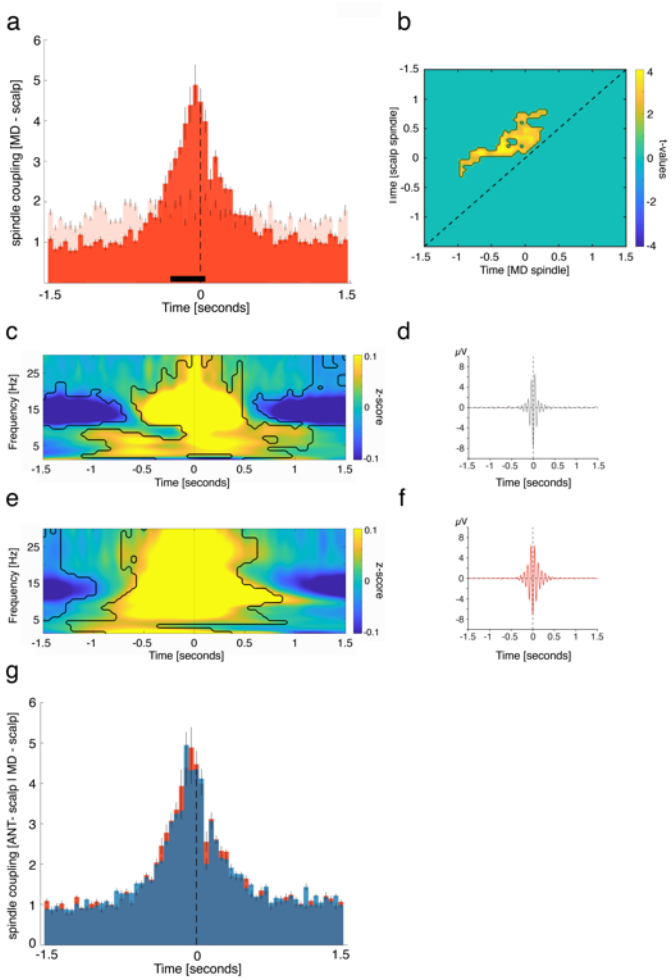

Fig 5. | MD spindles lead neocortical spindles. **(a)** Occurrence probabilities of MD spindle peaks relative to neocortical spindle peaks (maximal negative amplitude, time = 0; dashed line), indicating that MD spindles precede neocortical spindles. The solid black line indicates significant time bins, resulting from comparison with spindle-free control events (significant positive cluster from -0.3 to 0.05 sec, $p < 0.005$; corrected for multiple comparisons across time; time of peak: -0.05 sec). **(b)** Power-power correlations in the sleep spindle band for paired spindle events (locked to neocortical spindle peak), contrasted against event-free correlation maps. The contour lines indicate the significant cluster ($p = 0.002$, cluster corrected across time), showing that MD related spindle power precedes neocortical spindle power. **(c)** Time–frequency representation of neocortical spindles (locked to neocortical spindle peak), contrasted against event-free segments. The contour lines indicate significant clusters ($p < 0.05$, corrected for multiple comparisons across time and frequency). **(d)** Grand average EEG trace of neocortical spindles (mean ± SEM, maximally negative amplitude, time 0). **(e)** Time–frequency representation of all MD spindles (locked to MD spindle peak), contrasted against event-free segments. The contour lines indicate significant clusters ($p < 0.05$, corrected for multiple comparisons across time and frequency). **(f)** Grand average iEEG trace of MD spindles (mean ± SEM, maximally negative amplitude, time 0). **(g)** Direct comparison of ANT-neocortical and MD-neocortical interactions with regards to spindles yielded that the timing of ANT and MD-related spindles in relation to neocortical spindles was highly similar (cluster with lowest $p = 0.52$).

ANT spindles lock to early SO phases

So far, we established that both, neocortical SOs and spindles are preceded by corresponding activity in the ANT. These results also imply that the properties of local SO-spindle interactions, which are thought to shape memory consolidation [14,31], may differ between thalamic and neocortical sites, to allow for a concomitant thalamo-cortical coordination of SOs and spindles. To address this, we isolated SO-spindles complexes

in ANT as well as scalp recordings and extracted the onset latencies of spindles relative to their corresponding SO down states within both regions, respectively.

In line with previous findings [19,32], occurrence probabilities of neocortical spindles with respect to neocortical SOs (Fig. 6a), indicated that spindles started specifically at the SO down-to-up transition (0.05 to 0.15 s; $p < 0.0001$; peak: 0.1 sec). In contrast, ANT spindles preferential emerged around ANT SO down states (-0.15 to 0.25 s; $p = 0.0012$; peak: 0 s; Fig. 6b). These diverging dynamics also became apparent when depicting the SO-locked (down state) neocortical and ANT derived SO-spindle TFRs (Fig. 6c: locked to neocortical SO down state; Fig. 6d: locked to ANT SO down state). TFRs for both ANT and scalp derived SO-spindle complexes exhibited characteristic power-increases in the SO and sleep spindle band ($p < 0.05$, corrected for multiple comparisons across time and frequency). However, while neocortical spindles showed their typical power peaks well after the corresponding down states [1,16], increases in the ANT sleep spindle band were initiated around the ANT SO down states.

Finally, directly comparing the occurrence probabilities of thalamic and neocortical SO-spindle complexes affirmed that ANT spindles locked significantly earlier to SOs than neocortical spindles (-0.3 to -0.1, $p = 0.0039$; Fig. 6e). In a complementary analytical approach, we determined the preferred phase of SO-spindle modulation (i.e., SO-spindle coupling), for both ANT and neocortical events, respectively, by assessing the SO phases corresponding to the spindle onset latencies in each contact / scalp electrode. In 12/12 ANT contacts we found significant nonuniform distributions ($p < 0.05$, corrected for multiple comparisons using FDR; Rayleigh test, mean vector length: 0.41 ± 0.03) and a significant nonuniform distribution across contacts (Rayleigh $z = 9.33$, $p < 0.0001$), with spindles starting near the SO down state (corresponding to ± 180°; mean coupling direction: −175.22° ± 6.92°; see Fig. 6f). Similarly, we found in 7/8 scalp contacts a significant nonuniform distribution ($p < 0.05$, corrected for multiple comparisons using FDR; Rayleigh test, mean vector length: 0.27 ± 0.02). Again, a significant nonuniform distribution across participants was present (Rayleigh $z = 6.91$, $p < 0.0001$), with spindles preferentially starting at the SO down-to-up transition (mean coupling direction: −137.14 ± 7.58°; see Fig. 6f). Next, we tested whether the preferred coupling phases would vary systematically between ANT and neocortical areas, using the circular Watson-Williams test. Indeed, we found a significant difference in relation to the preferred phase of ANT and neocortical SO-spindle modulation ($F = 9.31$; $p = 0.0069$), corroborating the finding that spindles in the thalamus lock to earlier phases of the SO. Finally, we quantified the directional influence of SOs on spindles in both ANT and neocortical data, using the

phase-slope index [33,34]. We found that SOs predicted sleep spindle activity within ANT and neocortex, respectively, as evidenced by a positive PSI (ANT: 0.0040 ± 0.0017; t-test against zero: t = 2.37, p = 0.037; neocortex: 0.0048 ± 0.002; t-test against zero: t = 2.44, p = 0.044; Fig. 6g).

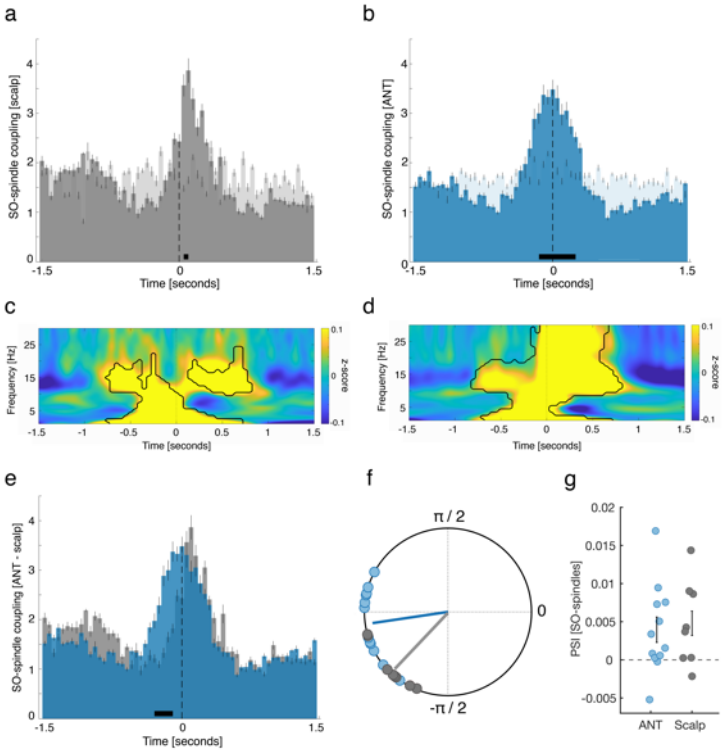

Fig 6. | ANT spindles lock to early SO phases. (a) Occurrence probabilities of neocortical spindle onsets with respect to neocortical SO down states, illustrating that spindles started specifically at the SO down-to-up transition (0.05 to 0.15 sec; p < 0.0001; peak: 0.1 sec). (b) ANT spindles preferential emerged around ANT SO down states (-0.15 to 0.25 sec; p = 0.0012; peak: 0 sec). (c) Time–frequency representation of neocortical SO-spindle events (locked to neocortical SO down state peaks), contrasted against event-free segments. The contour lines indicate significant clusters (p < 0.05, corrected for multiple comparisons across time and frequency). (d) Time–frequency representation of all ANT SO-spindle events (locked to ANT SO down state peaks), contrasted against event-free segments. The contour lines indicate significant clusters (p < 0.05, corrected for multiple comparisons across time and frequency). (e) Direct comparison of the occurrence probabilities of ANT and neocortical SO-spindle complexes yielded that ANT spindles locked significantly earlier to SOs as compared to neocortical spindles (-0.3 to -0.1, p = 0.0039). (f) Phases of the SO-spindle modulation derived from neocortical (gray circles) and ANT (blue circles) events. Neocortical spindle onsets preferentially emerged at the neocortical SO down-to-up transition (phase of neocortical SO down states corresponds to ± π; mean coupling direction: −137.14 ± 7.58°; Rayleigh z = 6.91, p < 0.0001), while ANT spindles started specifically around the ANT SO down states (mean coupling direction: −175.22° ± 6.92°; Rayleigh z = 9.33, p < 0.0001). The preferred phases of SO-spindle modulation differed significantly between the ANT and neocortical sites (Watson-Williams test: F = 9.31; p = 0.0069). (g) Directional SO-spindle coupling as obtained by the phase-slope index (PSI; mean ± SEM) for ANT (blue circles) and neocortical (gray circles) SO-spindle complexes. SO-phases significantly predicted spindle amplitudes both in case of ANT (t-test against zero: p = 0.037) and neocortical SO-spindle events (t-test against zero: p = 0.044).

MD spindles lock to early SO phases

We have shown that neocortical SOs precede MD SOs, while MD spindles lead neocortical spindles. Accordingly, the coupling within MD related SO-spindle complexes is expected to be shifted compared to neocortical SO-spindle complexes. Occurrence probabilities indicated that neocortical spindles started specifically at the down-to-up transition of neocortical SOs (0.1 to 0.3 s; $p = 0.003$; peak: 0.1 s; Fig 7a). MD spindles, however, started preferentially around the MD SO down states (-0.35 to 0 s; $p < 0.0001$; peak: -0.05 s; Fig 7b). Figures 7c and d show the neocortical and MD SO-spindle TFRs (Fig. 7c: locked to neocortical SO down states; Fig. 7d: locked to MD SO down state). TFRs for both scalp and MD derived SO-spindle complexes featured power-increases in the SO and sleep spindle band ($p < 0.05$, corrected for multiple comparisons across time and frequency). Neocortical spindles exhibited their typical power peaks after the corresponding down states, while power peaks of MD sleep spindles started around MD SO down states. Accordingly, the direct comparison of occurrence probabilities revealed that MD spindles locked significantly earlier to accompanying MD SOs as did neocortical spindles to neocortical SOs (-0.35 to 0.05, $p < 0.0001$; Fig. 7e).

Next, we determined the preferred phase of SO-spindle modulation for MD and neocortical events, respectively, by assessing the SO phases corresponding to the spindle onset latencies in each contact / scalp electrode. In 15/15 thalamic contacts, we found significant nonuniform distributions ($p < 0.05$, corrected for multiple comparisons using FDR; Rayleigh test, mean vector length: 0.42 ± 0.03). Also, across contacts the distribution was significantly nonuniform (Rayleigh $z = 12.10$, $p < 0.0001$), with spindles starting near the SO down state (corresponding to ± 180°; mean coupling direction: 172.26° ± 6.67°; see Fig. 7f).

For scalp derived data, we found in 9/11 contacts a significant nonuniform distribution ($p < 0.05$, corrected for multiple comparisons using FDR; Rayleigh test, mean vector length: 0.21 ± 0.02). Again, a significant nonuniform distribution across participants was present (Rayleigh $z = 8.18$, $p < 0.0001$), with spindles preferably starting at the down-to-up transition of neocortical SOs (mean coupling direction: −138.43 ± 9.05°; see Fig. 7f). When directly comparing the preferred coupling phases between MD and neocortical areas, we found a significant difference (Watson-Williams test: $F = 17.33$; $p = 0.0003$), supporting the outcome that spindles in the MD start at earlier phases of the SO then neocortical spindles. We also quantified the directional influence of SOs on spindles in both MD and neocortical data, using the phase-slope index [34,35]. Again, we show that SOs predicted sleep spindle activity within MD and neocortex, respectively, as evidenced

by a positive PSI (MD: 0.0016 ± 0.0006; t-test against zero: t = 2.36, p = 0.032; neocortex: 0.0028 ± 0.002; t-test against zero: t = 2.23, p = 0.049; Fig. 7g). Finally, we compared the features of ANT- and MD-derived SO-spindle complexes. While MD related sleep spindles had a tendency to lock to even earlier phases of MD related SOs (Fig. 7h), this difference was not significance (occurrence probabilities: p = 0.11; Fig. 7i: phase distribution: F = 1.29; p = 0.25).

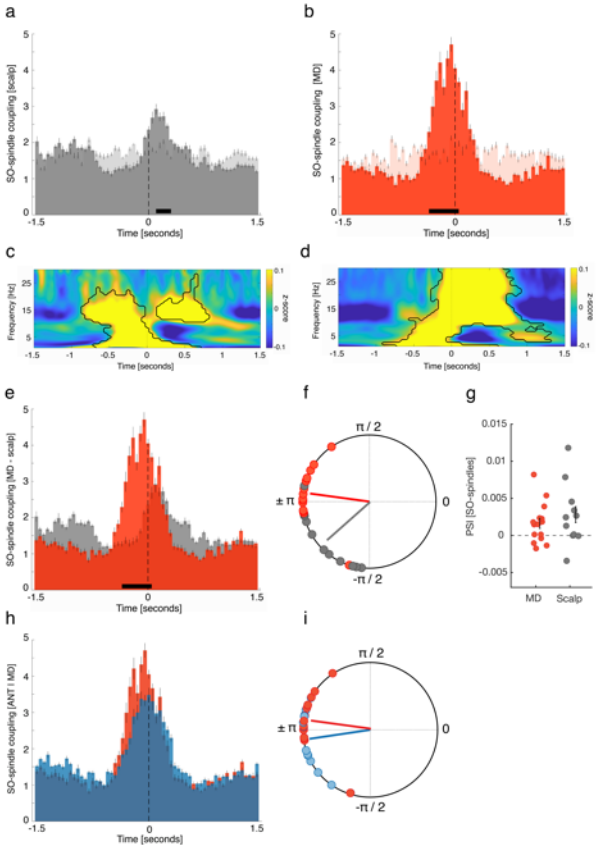

Fig7. | MD spindles lock to early SO phases. **(a)** Occurrence probabilities of neocortical spindle onsets with respect to neocortical SO down states, indicating that spindles started specifically at the SO down-to-up transition (0.05 to 0.15 sec; $p < 0.0001$; peak: 0.1 sec). **(b)** MD spindles started around MD SO down states (-0.35 to 0 sec; $p < 0.0001$; peak: -0.05 sec). **(c)** Time–frequency representation of neocortical SO-spindle events (locked to neocortical SO down state peaks), contrasted against event-free segments. The contour lines indicate significant clusters ($p < 0.05$, corrected for multiple comparisons across time and frequency). **(d)** Time–frequency representation of all MD SO-spindle events (locked to MD SO down state peaks), contrasted against event-free segments. The contour lines indicate significant clusters ($p < 0.05$, corrected for multiple comparisons across time and frequency). **(e)** Direct comparison of the occurrence probabilities of MD and neocortical SO-spindle complexes revealed that MD spindles start at significantly earlier SO phases as compared to neocortical spindles (-0.35 to 0.05, $p < 0.0001$). **(f)** Phases of the SO-spindle modulation derived from neocortical (gray circles) and MD (red circles) events. Neocortical spindle onsets preferentially emerged at the neocortical SO down-to-up transition (phase of neocortical SO down states corresponds to ± π; mean coupling direction: −138.43 ± 9.05°; Rayleigh z = 8.18, $p < 0.0001$), while MD spindles started specifically around the MD SO down states (mean coupling direction: 172.26 ± 6.67°; Rayleigh z = 12.10, $p < 0.0001$). The preferred phases of SO-spindle modulation differed significantly between the MD and neocortical sites (Watson-Williams test: F = 17.33; p = 0.0003). **(g)** Directional SO-spindle coupling obtained by the phase-slope index (PSI; mean ± SEM) for MD (red circles) and neocortical (gray circles) SO-spindle complexes. SO-phases significantly predicted spindle amplitudes both in case of MD (t-test against zero: p = 0.032) and neocortical SO-spindle events (t-test against zero: p = 0.049). **(h + i)** Directly comparing ANT- and MD-derived SO-spindle complexes did not yield a significant difference **(h)** occurrence probabilities: p = 0.11; **(i)** phase distribution: F = 1.29; p = 0.25).

DISCUSSION

Our results demonstrate a leading role of anterior thalamic activity in the orchestration of cardinal sleep rhythms in humans. In particular, we found that SOs recorded in the human ANT preceded their neocortical counterparts, in contrast to SOs recorded in the MD, which were led by neocortical SOs. Spindles recorded in ANT as well as MD preceded neocortical spindles. Finally, both in the ANT and the MD, thalamic spindles locked to early SO-phases, facilitating the prototypical synchrony between SOs and spindles in the neocortex.

Sleep oscillations have gained considerable interest over the last decade, mainly due their presumed role in facilitating the memory function of sleep [22]. SOs are thought to represent the time-giving pacemakers of memory consolidation and have been studied extensively in both rodent models and during human sleep [36,37]. Traditionally, they have been assumed to be solely generated within neocortical circuits [5,6]. However, recent animal studies cast doubt on this view by identifying essential thalamic contributions for SO generation and coordination [7–12]. Thalamic neurons have been shown to exhibit intrinsic, rhythmic up and down states in isolated conditions (i.e., without neocortical inputs [7,38]), while phasic burst-firing of thalamocortical neurons at the onset of up states often precedes the firing of neocortical neurons by 20 - 50 ms [9,39,40]. Optogenetic stimulation of thalamocortical neurons efficiently initiates neocortical up states [8,41]. In addition, thalamic activity terminates SO up states synchronously across neocortical areas, thus mediating a well-controlled down state transition [42]. In sum, these findings suggest that thalamic activity exerts a controlling influence on neocortical SOs, by coordinating up and down state dynamics in neocortical circuits. However, the generalization of thalamic contributions, and specifically of distinct thalamic nuclei, to sleep oscillations has been shown to be challenging across species (e.g., [43,44]), prompting their direct assessment during human sleep.

To investigate potential contributions of the ANT to neocortical SO coordination, we detected SOs during NREM sleep in intracranial contacts located in the ANT as well as scalp EEG. We show that the ANT not only exhibits a slow oscillatory rhythm (note that the ANT signal is likely to be of local origin due to a bipolar montage), but, importantly, that ANT SOs precede their neocortical counterparts. This might indicate that the ANT guides SO activity in the neocortex. Focusing on paired events only (i.e., time-windows where both neocortical and ANT SOs were present), we found that ANT SO phases significantly lead neocortical SO phases. Notably, this pattern of results was specific to ANT recordings. SOs in the MD did not precede but rather followed neocortical SOs,

which is in line with a previous report of neocortical SOs leading SOs in the human pulvinar [15]. Our findings thus highlight both a specific role of the ANT for SO dynamics and, more generally, the functional diversity of specific thalamic nuclei in humans [45].

What makes the ANT a favorable candidate for sculpting neocortical SOs? The ANT is a key node in the limbic circuit [46] and functionally relevant for human memory [24,25]. It has extensive connections with the anterior cingulate, orbitofrontal cortex and the hippocampus [47–49]. Notably, medial prefrontal regions, such as the orbitofrontal and the cingulate cortex have been identified as neocortical hot spots for the emergence of SO during human NREM sleep [50–52]. In addition, work in rodent models has shown that midline and anterior thalamic nuclei are likely candidates to influence global neocortical activity during sleep due to their widespread projections [9,42]. Hence, the dense connectivity of the ANT with medial prefrontal regions and within the limbic circuit sets the stage for ANT activity to shape neocortical SOs and coordinate sleep oscillations between regions implicated in memory consolidation.

We also found clear evidence for spindles in ANT and MD. Spindles emerge in recurrent loops between the thalamic nucleus reticularis (TRN) and thalamocortical neurons, which in turn forward them to the neocortex and hippocampus [26,53]. There have been conflicting findings across animal species about whether the TRN innervates the ANT and, hence, whether or not spindles are present in the ANT [23,43,44,54–58]. Our results provide a clear picture in humans: spindles are not only present both in the ANT and MD but also precede neocortical spindles, indicating an involvement of both nuclei in spindle generation and their projection to neocortical areas. In line with our interpretation, optogenetic stimulation of the rodent anterodorsal TRN, which innervates the ANT [44,56], has been shown to initiate spindles in the neocortex and hippocampus [59], indicating that the ANT might synchronize key areas of memory consolidation [27]. With regards to the MD it has been found that its neurons exhibit increased firing during spindle events [29] in rodents. In humans, reduced MD volume in persons with schizophrenia is associated with dampened neocortical spindle activity [60,61], further pointing towards a role of the MD in the thalamo-cortical spindle transfer. In sum, our results extend previous research identifying sleep spindles in other human thalamic nuclei [15,62], by showing that sleep spindles in the ANT and MD precede neocortical spindles during human sleep, indicating a role of both nuclei in thalamo-cortical spindle projections.

Finally, we set out to characterize the properties of SO-spindle interactions within the ANT and the MD. Spindles tend to nest within SO up states in scalp EEG recordings [14,32,63]. Importantly, the precise timing of neocortical spindle peaks with respect to the SO

upstate has been shown to be tightly linked to the behavioral expressions of memory consolidation [32,64,65]. Hence, the characteristics of SO-spindle interactions in the ANT might therefore highlight how the thalamus concomitantly groups SOs and spindles in the neocortex, leading to the well-known oscillatory nesting. We found that spindles in the ANT were initiated around the thalamic SO down state, in contrast to neocortical spindles that preferentially started later, at the neocortical SO down to up state transition (leading to the well-known nesting of neocortical spindles towards the up states) [3,63]. Thus, ANT spindles started at significantly earlier SO phases as compared to neocortical SO-spindle interactions. Notably, this divergent property of SO-spindle coordination is a necessary pre-requisite to allow for a concomitant coordination of neocortical SOs and spindles by the ANT. Specifically, while we show that both ANT SOs and spindles preceded their neocortical counterparts, the time lag between ANT and neocortical spindles exceeded the time lag between ANT and neocortical SOs. Hence, to enable the prototypical SO-spindle modulation in neocortical circuits (i.e., nesting of spindles towards the SO upstate) under the assumption that both graph-elements in the neocortex are governed by the ANT, it is inevitable that spindles start at relatively earlier phases of the SO in the ANT as compared to spindles of neocortical SO-spindle complexes.

We found a similar pattern of SO-spindle interactions within the MD, with spindles starting at early phases of the SO. Interestingly, even though not significant, spindles in the MD seem to start even earlier with respect to SOs as it is the case in the ANT. Again, in order to project spindles to the neocortex that nest in neocortical up states in a timely manner, a shifted coordination of SOs and spindles in the MD is necessary.

Taken together, our findings provide first evidence for the ANT as a major hub for coordinating the cardinal NREM-sleep related oscillations. In the neocortex, both spindles and SOs were led by ANT-related activity, while the interplay of local ANT SO-spindles was tuned in a way that allows for neocortical spindles to nest within SO up states. Importantly, this exact coordination is thought to be instrumental for the consolidation of memories [66,67].

Due to its projections to the medial prefrontal cortex and the hippocampus, the ANT has already been implicated in facilitating memory functioning and spatial navigation during wake, putatively by facilitating hippocampal-neocortical interactions [25,27,68–70]. Notably, the same hippocampal-cortical dialogue is assumed to underly sleep-related memory consolidation, facilitated by a precise coupling of hippocampal ripples, neocortical SOs and thalamic spindles [71]. The standard model suggests that neocortical SOs are imposed

448 on a rather passive thalamus, where they initiate spindles. Spindles in turn are thought to
449 synchronize hippocampal ripples and reactivated memory information [19,67]. Through this
450 coordination the reactivated memory information is suggested to arrive at the neocortex
451 during periods of high plasticity (i.e., during the presence of SO up states and spindles)
452 [72,73].

453 Our data critically extend these theoretical considerations, by spotlighting the human
454 thalamus, and in specific the ANT, as a putative active agent in interfacing sleep-related
455 oscillations between brain regions. While our current data remain agnostic with regards
456 to hippocampal activity, it has been shown in a single patient study, that hippocampal
457 spindles are aligned with SOs in the ANT [74]. Hence, ANT related oscillations might not
458 only migrate to the neocortex but likewise to the hippocampus, where spindles are known
459 to govern ripples and associated memory reactivation [66,75].Taken together, ANT related
460 activity might critically contribute to the triple coupling of sleep oscillations and thus, the
461 memory function of sleep. Future work will need to capture the association of ANT-
462 neocortical interactions with the behavioral expressions of memory consolidation, as well
463 as continue characterizing the functionally diverse human thalamus.
464
465

METHODS

Participants.

Intracranial and scalp EEG were simultaneously recorded from patients with bilateral depth electrodes implanted in the thalamus for deep brain stimulation (DBS) therapy of pharmaco-resistant epilepsy. Data was recorded at the Epilepsy Center, Department of Neurology, Ludwig-Maximilian Universität (Munich, Germany), while DBS leads were externalized post-surgery, prior to their connection to the pulse generator located in a subcutaneous infraclavicular or abdominal pouch [76]. The availability of direct iEEG recordings from the human thalamus is highly limited due to (i) the rarity of patients being treated with thalamic DBS, (ii) access to thalamic iEEG in these patients (post-surgery externalization of DBS leads is performed only in a fraction of these patients), and (iii) the limited amount of time for externalization (after surgery and before connecting the leads to the pulse generator).

A total of 13 patients participated. The data of 5 patients were discarded due to excessive epileptic activity. Out of the remaining 8 patients (mean age: 38.65 ± 3.59; 5 female), 6 patients contributed single full-night recordings, one patient contributed two consecutive full-night recordings and one patient contributed three consecutive full-night recordings. In sum, 11 full-night recordings entered the analyses of the present study. All patients received anticonvulsive medication (see Supplementary Table 7 and 8 for each participant's drug regimen at the time of recordings and their influence on sleep architecture). Informed consent was obtained from all patients. The study was approved by the ethics committee of the Medical Faculty of the Ludwig-Maximilian Universität.

Intracranial data acquisition and electrode localization

iEEG data was recorded from thalamic depth electrodes that each had four intracranial electrode contacts (platinum–iridium contacts, 1.5 mm wide with 1.5 mm edge-to-edge distance; Medtronic 3387). Data were recorded using XLTEK Neuroworks software (Natus Medical, San Carlos, California, US) and an XLTEK EMU128FS amplifier, with voltages referenced online to a CPz (250 Hz sampling rate in 7 patients; 200 Hz sampling rate in 1 patient).

The ANT in both hemispheres are the clinically-relevant implantation target for DBS therapy of epilepsy [77,78]. Due their small and high inter- and intraindividual variable size and the transventricular implantation trajectory, a subset of the electrode contacts ends up outside the ANT, frequently in the mediodorsal thalamus (see Fig. 1a).

The locations of the electrode contacts were estimated using the Lead-DBS toolbox [79]. First, the post-operative CT scan was co-registered to the pre-operative T1-weighted MRI, as implemented in the Advanced Normalisation Tools [80]. The scans were then spatially normalized to MNI space, based on the pre-operative T1 image using the unified segmentation approach as implemented in SPM12 [81]. Next, the trajectories of the DBS electrodes and positions of the electrode contacts were reconstructed based on the post-operative CT scan. The positions of the electrode contacts where then visually confirmed using the DISTAL atlas [82]. Based on this localization, the iEEG recordings were re-referenced to their immediate neighboring contact (bipolar montage). A bipolar pair of contacts was considered to be in the ANT if both or at least one contact was localized to the ANT, but no contact was localized in the MD. A bipolar pair of contacts was considered to be in the MD if both or at least one contact was localized to the MD, but no contact was localized in the ANT [83].

This procedure yielded 21 thalamic contacts (7 patients) in the ANT, and 24 contacts (8 patients) in the MD (see Supplementary Fig. 2 for a comparison of left and right ANT / MD contacts with regards to occurrence probabilities of SOs and spindles).

Scalp EEG acquisition

Scalp EEG was simultaneously recorded with iEEG via a common amplifier. Scalp EEG electrodes were placed on the accessible scalp according to the international 10-20 system for electrode placement. The sampling rate of the scalp EEG was identical to the sampling rate of the iEEG. Scalp EEG was recorded from 20 (2 patients), 22 (3 patients), 24 (1 patient) or 36 electrodes (2 patients). Scalp EEG was online referenced to CPz. Scalp EEG data was re-referenced offline against the mean of all available artifact-free scalp EEG electrodes.

Sleep staging

All available scalp electrodes were low-pass filtered at 40 Hz, down-sampled to 200 Hz (if necessary). Sleep staging was carried out according to standard criteria [84]. For subsequent analyses, sleep stages N2 and N3 were collapsed and referred to as non-rapid eye movement (NREM) sleep.

Data pre-processing

iEEG and scalp EEG were manually inspected to discard noisy or artefact-contaminated (e.g., excessive movements during NREM) channels (see below for detection of epileptic

activity). All data were down-sampled to 200 Hz, demeaned and de-trended. The recordings were then filtered using a 150 Hz Butterworth low-pass filter and a two Butterworth band-stop filters (to attenuate line noise; 48-52 Hz).

Interictal epileptic discharge (IED) detection: Epileptic activity in scalp and thalamic recordings was semi-automatically detected. First, interictal epileptic discharges were detected automatically by high- and low pass filtering the data below 20 and above 80 Hz and z-scoring the data. Subsequently, data segments with amplitudes exceeding the mean signal by 6 SDs for less than 100 ms [85,86] were identified. Second, iEEG and scalp EEG data was visually inspected for epileptic activity by two investigators, independently. Data segments comprising epileptic events at any given channel were discarded (13.91 ± 2.41 % of all sleep data). Four thalamic contacts (2 ANT contacts, 2 MD contacts) and on average 7.5 ± 0.92 scalp electrodes were discarded.

Event detection

SOs and sleep spindles were identified for each patient, based on established detection algorithms [19,32].

SO detection: Data were filtered between 0.3–2 Hz (two-pass FIR bandpass filter, order = three cycles of the low frequency cut-off). Only movement-free data (as determined during sleep scoring) from NREM sleep stages 2 and 3 were considered. All zero-crossings were determined in the filtered signal of each channel (iEEG and scalp EEG, respectively), and event duration was determined for SO candidates (that is, down states followed by up states) as time between two successive positive- to-negative zero-crossings. Events that met the SO duration criteria (minimum of 0.8 and maximum of 2 sec) and exceeded the mean amplitude of all detected events by 1.25 SD entered the analysis. For subsequent time-locked analyses (ERPs, time-frequency representations, etc.), 5-sec-long segments centered on the down state (± 2.5 sec) were extracted from the unfiltered raw signal.

Spindle detection: Data was filtered between 11–16 Hz (two-pass FIR bandpass filter, order = three cycles of the low frequency cut-off). Again, only artifact-free data from NREM sleep stages 2 and 3 were used for event detection. The root mean square (RMS) signal was calculated for the filtered signal at each channel using a moving average of 200 ms, and spindles that exceeded the mean amplitude of all detected events by 1.5 SD entered the analysis. Whenever the signal exceeded this threshold for more than 0.5 sec but less than 3 sec (duration criteria), a spindle event was detected. Epochs time-

locked to the maximally negative spindle trough (–2.5 to +2.5 sec) were extracted from the unfiltered raw signal for subsequent time-locked analyses.

SO-spindle complexes: To isolate SO-spindle complexes in scalp and thalamic recordings, we determined for all SOs whether a spindle was detected following the SO (SO down state + 750 ms). Again, SO-spindle events were extracted (–2.5 to +2.5 sec with regards to the SO down state) from the raw signal for subsequent time-locked analyses.

Paired events: To identify paired SO events (scalp & thalamus), we determined for all scalp detected SOs whether corresponding SOs were detectable in thalamic recordings within a time-window of ± 750 ms. Data segments locked to the scalp detected down states (± 2.5 sec) were extracted. Likewise, paired sleep spindles were isolated by determining for all scalp detected sleep spindles whether related spindles emerged (± 750 ms) in thalamic recordings. Data segments locked to the scalp detected maximally negative spindle peak (± 2.5 sec) were extracted.

Electrode selection [scalp EEG]: As outlined above, all electrodes exhibiting significant epileptic activity were discarded to ensure that our results were not influenced by epileptiform activity. This conservative procedure together with restricted access to the scalp due to post-surgical wound care impeded us from using identical scalp EEG electrodes across patients to delineate thalamo-cortical interactions during sleep (e.g., electrode Fz for SO related and electrode Cz for sleep spindle related analyses [18,19]. Instead, we pursued a data-driven and individualized approach. For SO-related analyses, we selected for each participant the frontal scalp electrode that exhibited the highest number of associated thalamic SOs within a time of ± 750 ms. This procedure was accomplished independently for data stemming from the ANT and the MD. The respective scalp electrodes (one related to the ANT, one related to the MD) were used for all subsequent SO-related analyses (see Supplementary Table 1 for on overview of the selected scalp electrode; see Supplementary Fig. 3 for ANT SO occurrence probabilities relative to scalp electrode Fz). Similarly, for sleep spindle related analyses, we selected the frontal, central or parietal scalp electrode that exhibited the highest number of associated thalamic spindles (ANT or MD, respectively; see Supplementary Table 2 for on overview of the selected scalp electrodes; see Supplementary Fig. 4 for spindle-spindle occurrence probabilities, were scalp spindles were exclusively derived from frontal or parietal electrodes). The respective scalp electrodes (one related to the

ANT, one related to the MD) were subsequently used for all sleep spindle-related analyses. Data from scalp electrodes was used as a proxy of neocortical activity.

Event-free segments: For statistical comparisons, we extracted 5-sec-long intervals during NREM sleep, which did not exhibit any SO, spindle or SO-spindle event, respectively. In each participant and electrode, the number of control events corresponded to the number of prior detected events of interest. Event-free events were only drawn from time window starting 5 mins before and ending 5 mins after the corresponding oscillatory event.

Analyses

Temporal relation between sleep oscillations: To assess the temporal relationship between scalp- and thalamus-derived SO events, we created peri-event time histograms (bin size = 50 ms) where scalp detected SO down states served as seed (time = 0), while the targets (thalamic SO down states) are depicted relative to the seed. The resulting histogram was normalized by the total number of detected scalp SOs (multiplied by 100). Similarly, for sleep spindles, peri-event histograms (bin size = 50 ms) of thalamic sleep spindle peaks (maximally negative amplitude) in relation to scalp sleep spindles peaks (maximally negative amplitude: ± 1.5 sec) were created. The resulting histogram was normalized by the total number of detected scalp spindles (multiplied by 100). To determine the interplay of SOs and sleep spindles (separately within scalp and thalamic recording), a peri-event histogram of sleep spindles (onsets) around SO down states (± 1.5 sec) was created. The resulting histogram was normalized by the total number of detected spindles (multiplied by 100). The same procedure was applied to spindle-free control segments.

Phase relationship between sleep oscillations: To estimate the phase-relationship between scalp and thalamic SOs, data epochs including paired events were filtered in the SO range (0.3–2 Hz, two-pass Butterworth bandpass filter). As described above, these segments included both scalp and thalamic SOs, and were time-locked to the down states of scalp detected SOs. A Hilbert transform was applied to the data and the instantaneous phase angle of the thalamic recording at the time of the scalp SO down state was extracted. Each participant's preferred phase of SO-SO coupling was then obtained by taking the circular mean of all individual events' preferred phases.

For the analysis of SO-spindle coupling, we filtered the SO-spindle data (locked to spindle onsets) in the SO range (0.3–2 Hz, two-pass Butterworth bandpass filter), applied a Hilbert transform and extracted the instantaneous phase angle. Next, we isolated the SO phase angle at the time of spindle onsets. Each participant's t preferred SO phase at spindle onsets was obtained by taking the circular mean of all individual events' preferred phases.

Spindle related across-channel power correlations: We further estimated the temporal relationship of thalamic and scalp detected spindles using channel to channel correlations of oscillatory power in the sleep spindle band. To this end, a Hanning window was applied to paired sleep spindles segments (locked to scalp detected maximally negative amplitude) and power values between 11 and 16 Hz were extracted for each time-bin. Power values were z-scored per channel and averaged. Subsequently, power values derived from thalamic channels were correlated with scalp related power values at each time-point (Spearman correlation), resulting in a 2d correlation map per contact pair. Finally, the correlation maps were normalized using the Fisher z-transform. The same procedure was applied to spindle-free control segments. Off-diagonal correlations indicate a time-lag between spindle power in scalp and thalamic channels.

Phase Slope Index: We assessed whether SOs drive activity in the sleep spindle range or vice versa in NREM sleep data segments comprising SO-spindle complexes, separately for thalamic and scalp recordings. The cross-frequency phase-slope index [34,] was calculated for each contact between the signal and the signal filtered in the sleep spindle range (11 – 16 Hz). After applying a Hanning window and extracting the complex Fourier coefficients, all SO frequencies < 2 Hz were considered. In this context, positive values indicate SOs driving sleep spindle activity, while negative values indicate sleep spindles driving SOs. The obtained data distributions were tested against zero, using paired samples t-tests.

Time frequency representations: Time–frequency analyses of SO, sleep spindle and SO-spindle segments were performed using FieldTrip [87]. Frequency decomposition of the data was achieved using Fourier analysis based on sliding time windows (moving forward in 50 ms increments). The window length was set to five cycles of a given frequency (frequency range: 1–30 Hz in 1 Hz steps). The windowed data segments were multiplied with a Hanning taper before Fourier analysis [–2.5 to 2.5 sec]. The longer time segments

were chosen to allow for resolving low frequency activity within the time windows of interest [–1.5 to 1.5 sec] and avoid edge artifacts. Resulting power values were z-scored across time. The same procedure was applied to event-free control segments.

Statistics: Statistical analyses were performed at the individual electrodes / contacts level (fixed-effects analysis), considering all electrodes / contacts that were eligible based on our criteria (e.g., artefact free, etc.). Unless stated otherwise, we used cluster-based permutation tests to correct for multiple comparisons as implemented in fieldtrip. A dependent-samples t-test was used at the sample level and values were thresholded at p = 0.05 (1000 randomizations). The sum of all t-values in cluster served as cluster statistic and Monte Carlo simulations were used to calculate the cluster p-value (alpha = 0.05, two-tailed) under the permutation distribution. The input data were either occurrence probabilities across time (e.g., Fig. 2a), time x frequency values (e.g., Fig. 2c) or time x time correlation maps (e.g., Fig. 4b) which were tested against corresponding data stemming from event-free events. In case of between area comparisons (e.g., Fig. 3g) independent samples t-tests (cluster corrected) were employed to conform with the varying number of observation units (i.e., contacts).

For circular statistics the phase distributions (within or across participants) were tested against uniformity using the Rayleigh test (CircStat toolbox [88]). When directly comparing phase distributions across recording sites, the circular Watson-Williams test was used [88,89].

References:

1. Mölle, M., Bergmann, T. O., Marshall, L. & Born, J. Fast and slow spindles during the sleep slow oscillation: disparate coalescence and engagement in memory processing. *Sleep* **34**, 1411–21 (2011).
2. Piantoni, G. *et al.* Modulation of gamma and spindle-range power by slow oscillations in scalp sleep EEG of children. *Int. J. Psychophysiol.* (2013). doi:10.1016/j.ijpsycho.2013.01.017
3. Klinzing, J. G., Niethard, N. & Born, J. Mechanisms of systems memory consolidation during sleep. *Nature Neuroscience* (2019). doi:10.1038/s41593-019-0467-3
4. Amzica, F. & Steriade, M. The functional significance of K-complexes. *Sleep Med. Rev.* **6**, 139–149 (2002).
5. Steriade, M., McCormick, D. A. & Sejnowski, T. J. Thalamocortical oscillations in the sleeping and aroused brain. *Science (80-.).* (1993). doi:10.1126/science.8235588
6. Timofeev, I., Grenier, F., Bazhenov, M., Sejnowski, T. J. & Steriade, M. Origin of slow cortical oscillations in deafferented cortical slabs. *Cereb. Cortex* (2000). doi:10.1093/cercor/10.12.1185
7. Hughes, S. W., Cope, D. W., Blethyn, K. L. & Crunelli, V. Cellular Mechanisms of the Slow (. *Neuron* (2002).
8. David, F. *et al.* Essential thalamic contribution to slow waves of natural sleep. *J. Neurosci.* (2013). doi:10.1523/JNEUROSCI.3169-13.2013
9. Gent, T. C., Bandarabadi, M., Herrera, C. G. & Adamantidis, A. R. Thalamic dual control of sleep and wakefulness. *Nat. Neurosci.* (2018). doi:10.1038/s41593-018-0164-7
10. Crunelli, V. & Hughes, S. W. The slow (<1 Hz) rhythm of non-REM sleep: a dialogue between three cardinal oscillators. *Nat. Neurosci.* **13**, 9 (2010).
11. Crunelli, V., David, F., Lorincz, M. L. & Hughes, S. W. The thalamocortical network as a single slow wave-generating unit. *Curr. Opin. Neurobiol.* **31**, 72–80 (2015).
12. Neske, G. T. The Slow Oscillation in Cortical and Thalamic Networks: Mechanisms and Functions. *Front. Neural Circuits* **9**, (2016).
13. Steriade, M. Grouping of brain rhythms in corticothalamic systems. *Neuroscience* **137**, 1087–1106 (2006).
14. Helfrich, R. F., Mander, B. A., Jagust, W. J., Knight, R. T. & Walker, M. P. Old Brains Come Uncoupled in Sleep: Slow Wave-Spindle Synchrony, Brain Atrophy, and Forgetting. *Neuron* **97**, 221-230.e4 (2018).
15. Mak-McCully, R. A. *et al.* Coordination of cortical and thalamic activity during non-REM sleep in humans. *Nat. Commun.* **8**, 15499 (2017).
16. Mölle, M., Marshall, L., Gais, S. & Born, J. Grouping of spindle activity during slow oscillations in human non-rapid eye movement sleep. *J. Neurosci.* **22**, 10941–7 (2002).
17. Sirota, A., Csicsvari, J., Buhl, D. & Buzsáki, G. Communication between neocortex and hippocampus during sleep in rodents. *Proc. Natl. Acad. Sci. U. S. A.* **100**, 2065–2069 (2003).
18. Clemens, fia *et al.* Temporal coupling of parahippocampal ripples, sleep spindles and slow oscillations in humans. doi:10.1093/brain/awm146
19. Staresina, B. P. *et al.* Hierarchical nesting of slow oscillations, spindles and ripples in the human hippocampus during sleep. *Nat. Neurosci.* **18**, 1679–1686 (2015).
20. Rasch, B. & Born, J. About sleep's role in memory. *Physiol. Rev.* **93**, 681–766 (2013).

21. Schreiner, T. & Staudigl, T. Electrophysiological signatures of memory reactivation in humans. *Philosophical Transactions of the Royal Society B: Biological Sciences* **375**, (2020).
22. Girardeau, G. & Lopes-dos-Santos, V. Brain neural patterns and the memory function of sleep. *Science (80-.).* **374**, 560–564 (2021).
23. Pergola, G. *et al.* The Regulatory Role of the Human Mediodorsal Thalamus. *Trends Cogn. Sci.* **22**, 1011–1025 (2018).
24. Aggleton, J. P., Pralus, A., Nelson, A. J. D. & Hornberger, M. Thalamic pathology and memory loss in early Alzheimer's disease: moving the focus from the medial temporal lobe to Papez circuit. *Brain* **139**, 1877–1890 (2016).
25. Aggleton, J. P. & Brown, M. W. Episodic memory, amnesia, and the hippocampal–anterior thalamic axis. *Behav. Brain Sci.* **22**, 425–444 (1999).
26. Fernandez, L. M. J. & Lüthi, A. Sleep Spindles: Mechanisms and Functions. *Physiological reviews* **100**, 805–868 (2020).
27. Viejo, G. & Peyrache, A. Precise coupling of the thalamic head-direction system to hippocampal ripples. *Nat. Commun. 2020 111* **11**, 1–14 (2020).
28. Varela, C. & Wilson, M. A. Mpfc spindle cycles organize sparse thalamic activation and recently active ca1 cells during non-rem sleep. *Elife* (2020). doi:10.7554/eLife.48881
29. Yang, M., Logothetis, N. K. & Eschenko, O. Occurrence of Hippocampal Ripples is Associated with Activity Suppression in the Mediodorsal Thalamic Nucleus. *J. Neurosci.* (2019). doi:10.1523/jneurosci.2107-18.2018
30. Benjamini, Y. & Hochberg, Y. Controlling the False Discovery Rate: A Practical and Powerful Approach to Multiple Testing. *Source J. R. Stat. Soc. Ser. B* **57**, 289–300 (1995).
31. Hahn, M. A., Heib, D., Schabus, M., Hoedlmoser, K. & Helfrich, R. F. Slow oscillation-spindle coupling predicts enhanced memory formation from childhood to adolescence. *Elife* **9**, 1–21 (2020).
32. Schreiner, T., Petzka, M., Staudigl, T. & Staresina, B. P. Endogenous memory reactivation during sleep in humans is clocked by slow oscillation-spindle complexes. *Nat. Commun.* (2021). doi:10.1038/s41467-021-23520-2
33. Nolte, G. *et al.* Robustly estimating the flow direction of information in complex physical systems. *Phys. Rev. Lett.* **100**, 234101 (2008).
34. Jiang, H., Bahramisharif, A., van Gerven, M. A. J. & Jensen, O. Measuring directionality between neuronal oscillations of different frequencies. *Neuroimage* **118**, 359–367 (2015).
35. Marzetti, L., Del Gratta, C. & Nolte, G. Understanding brain connectivity from EEG data by identifying systems composed of interacting sources. *Neuroimage* **42**, 87–98 (2008).
36. Mölle, M. & Born, J. Slow oscillations orchestrating fast oscillations and memory consolidation. **193**, 93–110 (2011).
37. Adamantidis, A. R., Gutierrez Herrera, C. & Gent, T. C. Oscillating circuitries in the sleeping brain. *Nat. Rev. Neurosci.* **20**, 746–762 (2019).
38. Blethyn, K. L., Hughes, S. W., Tóth, T. I., Cope, D. W. & Crunelli, V. Neuronal Basis of the Slow (<1 Hz) Oscillation in Neurons of the Nucleus Reticularis Thalami In Vitro. *J. Neurosci.* **26**, 2474–2486 (2006).
39. Contreras, D. & Steriade, M. Cellular basis of EEG slow rhythms: a study of dynamic corticothalamic relationships. *J. Neurosci.* **15**, 604–22 (1995).
40. Slézia, A., Hangya, B., Ulbert, I. & Acsády, L. Phase Advancement and Nucleus-Specific Timing of Thalamocortical Activity during Slow Cortical Oscillation. *J. Neurosci.* **31**, 607–617 (2011).
41. Poulet, J. F. A., Fernandez, L. M. J., Crochet, S. & Petersen, C. C. H. Thalamic

control of cortical states. *Nat. Neurosci. 2012 153* **15**, 370–372 (2012).

42. Hay, Y. A. *et al.* Thalamus mediates neocortical Down state transition via GABA B-receptor-targeting interneurons. *Neuron* **109**, 2682-2690.e5 (2021).
43. Pare, D., Steriade, M., Deschenes, M. & Oakson, G. Physiological characteristics of anterior thalamic nuclei, a group devoid of inputs from reticular thalamic nucleus. *https://doi.org/10.1152/jn.1987.57.6.1669* **57**, 1669–1685 (1987).
44. Gonzalo-Ruiz, A. & Lieberman, A. R. Topographic organization of projections from the thalamic reticular nucleus to the anterior thalamic nuclei in the rat. *Brain Res. Bull.* **37**, 17–35 (1995).
45. Halassa, M. M. & Sherman, S. M. Thalamocortical Circuit Motifs: A General Framework. *Neuron* **103**, 762–770 (2019).
46. Jankowski, M. M. *et al.* The anterior thalamus provides a subcortical circuit supporting memory and spatial navigation. *Front. Syst. Neurosci.* **7**, (2013).
47. Grodd, W., Kumar, V. J., Schüz, A., Lindig, T. & Scheffler, K. The anterior and medial thalamic nuclei and the human limbic system: tracing the structural connectivity using diffusion-weighted imaging. *Sci. Reports 2020 101* **10**, 1–25 (2020).
48. Van Groen, T. & Wyss, J. M. Projections from the anterodorsal and anteroveniral nucleus of the thalamus to the limbic cortex in the rat. *J. Comp. Neurol.* **358**, 584–604 (1995).
49. Hicks, R. R. & Huerta, M. F. Differential thalamic connectivity of rostral and caudal parts of cortical area Fr2 in rats. *Brain Res.* **568**, 325–329 (1991).
50. Massimini, M., Huber, R., Ferrarelli, F., Hill, S. & Tononi, G. The sleep slow oscillation as a traveling wave. *J. Neurosci.* **24**, 6862–70 (2004).
51. Nir, Y. *et al.* Regional Slow Waves and Spindles in Human Sleep. *Neuron* **70**, 153–169 (2011).
52. Riedner, B. A., Hulse, B. K., Murphy, M. J., Ferrarelli, F. & Tononi, G. Temporal dynamics of cortical sources underlying spontaneous and peripherally evoked slow waves. *Prog. Brain Res.* **193**, 201–218 (2011).
53. De Gennaro, L. & Ferrara, M. Sleep spindles: an overview. *Sleep Med. Rev.* **7**, 423–440 (2003).
54. Steriade, M. & Deschenes, M. The thalamus as a neuronal oscillator. *Brain Res.* **320**, 1–63 (1984).
55. Halassa, M. M. & Acsády, L. Thalamic Inhibition: Diverse Sources, Diverse Scales. *Trends Neurosci.* **39**, 680–693 (2016).
56. Gentet, L. J. & Ulrich, D. Strong, reliable and precise synaptic connections between thalamic relay cells and neurones of the nucleus reticularis in juvenile rats. *J. Physiol.* **546**, 801–811 (2003).
57. Zikopoulos, B. & Barbas, H. Parallel driving and modulatory pathways link the prefrontal cortex and thalamus. *PLoS One* **2**, (2007).
58. Velayos, J. L., Oliva, M. & Alfageme, F. Afferent projections to the mediodorsal and anterior thalamic nuclei in the cat. Anatomical-clinical correlations. *Brain Pathol.* **8**, 549–552 (1998).
59. Latchoumane, C.-F. V., Ngo, H.-V. V., Born, J. & Shin, H.-S. Thalamic Spindles Promote Memory Formation during Sleep through Triple Phase-Locking of Cortical, Thalamic, and Hippocampal Rhythms. *Neuron* 1–12 (2017). doi:10.1016/j.neuron.2017.06.025
60. Buchmann, A. *et al.* Reduced mediodorsal thalamic volume and prefrontal cortical spindle activity in schizophrenia. *Neuroimage* **102 Pt 2**, 540–547 (2014).
61. Ferrarelli, F. & Tononi, G. Reduced sleep spindle activity point to a TRN-MD thalamus-PFC circuit dysfunction in schizophrenia. *Schizophr. Res.* **180**, 36–43 (2017).

62. Bastuji, H., Lamouroux, P., Villalba, M., Magnin, M. & Garcia-Larrea, L. Local sleep spindles in the human thalamus. *J. Physiol.* **598**, 2109–2124 (2020).
63. Mölle, M., Marshall, L., Gais, S. & Born, J. Grouping of spindle activity during slow oscillations in human non-rapid eye movement sleep. *J. Neurosci.* **22**, 10941–10947 (2002).
64. Mikutta, C. *et al.* Phase-amplitude coupling of sleep slow oscillatory and spindle activity correlates with overnight memory consolidation. *J. Sleep Res.* **28**, (2019).
65. Zhang, J., Yetton, B., Whitehurst, L. N., Naji, M. & Mednick, S. C. The effect of zolpidem on memory consolidation over a night of sleep. *Sleep* (2020). doi:10.1093/sleep/zsaa084
66. Kim, J., Gulati, T. & Ganguly, K. Competing Roles of Slow Oscillations and Delta Waves in Memory Consolidation versus Forgetting. *Cell* **179**, 514-526.e13 (2019).
67. Maingret, N., Girardeau, G., Todorova, R., Goutierre, M. & Zugaro, M. Hippocampo-cortical coupling mediates memory consolidation during sleep. *Nat. Neurosci.* **19**, 959–964 (2016).
68. Taube, J. S. Head direction cells recorded in the anterior thalamic nuclei of freely moving rats. *J. Neurosci.* **15**, 70–86 (1995).
69. Peyrache, A., Lacroix, M. M., Petersen, P. C. & Buzsáki, G. Internally organized mechanisms of the head direction sense. *Nat. Neurosci.* **18**, 569–575 (2015).
70. Leszczyński, M. & Staudigl, T. Memory-guided attention in the anterior thalamus. *Neurosci. Biobehav. Rev.* **66**, 163–165 (2016).
71. Diekelmann, S. & Born, J. The memory function of sleep. *Nat. Rev. Neurosci.* **11**, 114–126 (2010).
72. Niethard, N., Ngo, H. V. V., Ehrlich, I. & Born, J. Cortical circuit activity underlying sleep slow oscillations and spindles. *Proc. Natl. Acad. Sci. U. S. A.* (2018). doi:10.1073/pnas.1805517115
73. Seibt, J. *et al.* Cortical dendritic activity correlates with spindle-rich oscillations during sleep in rodents. *Nat. Commun.* **8**, (2017).
74. Sarasso, S. *et al.* Hippocampal sleep spindles preceding neocortical sleep onset in humans. *Neuroimage* **86**, 425–432 (2014).
75. Ngo, H.-V. V, Fell, J. & Staresina, B. P. Sleep spindles mediate hippocampal-neocortical coupling during sharp-wave ripples. *bioRxiv* 712463 (2019). doi:10.1101/712463
76. Kaufmann, E., Bötzel, K., Vollmar, C., Mehrkens, J. H. & Noachtar, S. What have we learned from 8 years of deep brain stimulation of the anterior thalamic nucleus? Experiences and insights of a single center. *J. Neurosurg.* **135**, 619–628 (2020).
77. Fisher, R. *et al.* Electrical stimulation of the anterior nucleus of thalamus for treatment of refractory epilepsy. *Epilepsia* (2010). doi:10.1111/j.1528-1167.2010.02536.x
78. Kaufmann, E. *et al.* European Expert Opinion on ANT-DBS therapy for patients with drug-resistant epilepsy (a Delphi consensus). *Seizure* (2020). doi:10.1016/j.seizure.2020.08.015
79. Horn, A. & Kühn, A. A. Lead-DBS: a toolbox for deep brain stimulation electrode localizations and visualizations. *Neuroimage* **107**, 127–135 (2015).
80. Avants, B. B., Epstein, C. L., Grossman, M. & Gee, J. C. Symmetric diffeomorphic image registration with cross-correlation: evaluating automated labeling of elderly and neurodegenerative brain. *Med. Image Anal.* **12**, 26–41 (2008).
81. Ashburner, J. & Friston, K. J. Unified segmentation. *Neuroimage* **26**, 839–851 (2005).

82. Ewert, S. *et al.* Toward defining deep brain stimulation targets in MNI space: A subcortical atlas based on multimodal MRI, histology and structural connectivity. *Neuroimage* **170**, 271–282 (2018).
83. Deutschová, B. *et al.* Thalamic oscillatory activity may predict response to deep brain stimulation of the anterior nuclei of the thalamus. *Epilepsia* (2021). doi:10.1111/epi.16883
84. Iber, C., Ancoli-Israel, S., Chesson, A. & Quan, S. *The AASM Manual for the Scoring of Sleep and Associated Events: Rules, Terminology, and Technical Specification. American Academy of Sleep Medicine* (2007).
85. Andrillon, T. *et al.* Sleep spindles in humans: insights from intracranial EEG and unit recordings. *J. Neurosci.* **31**, 17821–17834 (2011).
86. Helfrich, R. F. *et al.* Bidirectional prefrontal-hippocampal dynamics organize information transfer during sleep in humans. *Nat. Commun.* (2019). doi:10.1038/s41467-019-11444-x
87. Oostenveld, R., Fries, P., Maris, E. & Schoffelen, J.-M. FieldTrip: Open source software for advanced analysis of MEG, EEG, and invasive electrophysiological data. *Comput. Intell. Neurosci.* **2011**, 156869 (2011).
88. Berens, P. CircStat: A MATLAB toolbox for circular statistics. *J. Stat. Softw.* **31**, 1–21 (2009).
89. VanRullen, R. How to Evaluate Phase Differences between Trial Groups in Ongoing Electrophysiological Signals. *Front. Neurosci.* **10**, (2016).

Acknowledgments

This work was supported by the European Research Council (https://erc.europa.eu/, Starting Grant 802681 awarded to TSt). We are indebted to all patients who volunteered to participate in this study. We thank the staff and physicians of the at the Epilepsy Center, Department of Neurology, Ludwig Maximilians University, Munich for assistance.

Author Contributions

Conceptualization: TS, TSt; Resources: EK, NS, JHM; Formal Analysis: TS, TSt; Funding acquisition: TSt; Writing – original draft: TS, TSt; Writing– review & editing: TS, TSs, EK, SN

Corresponding author

Correspondence to Tobias Staudigl

Competing interests

The authors declare no competing interests.

Supplementary Information for:

The human thalamus orchestrates neocortical oscillations during NREM sleep.

Thomas Schreiner[1], Elisabeth Kaufmann[2], Soheyl Noachtar[2], Jan-Hinnerk Mehrkens[3] & Tobias Staudigl[1]

1 Department of Psychology, Ludwig-Maximilians-Universität München, Munich, Germany

2 Epilepsy Center, Department of Neurology, Ludwig-Maximilians-Universität München, Munich, Germany

3 Department of Neurosurgery, Ludwig-Maximilians-Universität München, Munich, Germany

Supplementary tables

Supplementary Table 1 | Sleep architecture: Data are means ± s.e.m. N1, N2: NREM sleep stages N1 & N2, SWS: slow-wave sleep, REM: rapid eye movement sleep, WASO: wake after sleep onset. TST: total sleep time (in minutes).

	N1	N2	SWS	REM	WASO	TST [min]
Sleep stage [%]	6.1 ± 1.7	47.4 ± 4.2	16.5 ± 3.5	12.7 ± 2.2	15.9 ± 3.5	529.4 ± 30.1

Supplementary Table 2 | scalp electrodes: overview of scalp electrode that were selected for the respective analyses.

	ANT-SO	ANT-spindle	MD-SO	MD-spindle
P1	Fz	Fp1	Fz	P4
P2	F4	F4	FP2	Pz
P3	F8	F4	F4	F4
P4	FT10	Pz	FT10	C3
P5	F4	Pz	F3	P3
P6	Fz	C3	Fz	Pz
P7	FT10	C4	Fz	Pz
P8	-	-	F7	Cz

Supplementary Table 3 | Sleep Oscillations ANT: Data are means ± s.e.m. Number of detected events and percentage of paired events in NREM sleep at ANT contacts and scalp electrodes.

	ANT	Scalp	t	*P*
SO number	1573.8 ± 129.9	1513.5 ± 130.1	1.11	0.29
SO-coupling [%]	33.74 ± 3.02	31.11 ± 3.25	2.07	0.06
spindle number	2203.8 ± 213.5	1903.3 ± 211.5	3.19	0.008
spindle-coupling [%]	43.8 ± 4.2	37.3 ± 4.1	3.43	0.005
SO-spindle number	431 ± 52.1	304.1 ± 69.8	3.18	0.008

Supplementary Table 4 | Sleep Oscillations MD: Data are means ± s.e.m. Number of detected events and percentage of paired events in NREM sleep at MD contacts and scalp electrodes.

	MD	Scalp	t	*P*
SO number	1408.5 ± 126.2	1476.9 ± 129.1	1.06	0.31
SO-coupling [%]	30.45 ± 2.31	29.51 ± 3.15	1.37	0.35
Spindle number	2172.8 ± 238.2	1796.5 ± 229.8	3.35	0.005
spindle-coupling [%]	45.1 ± 5.5	30.2 ± 4.6	2.18	0.046
SO-spindle number	488 ± 53.5	338.5 ± 79.7	1.78	0.095

Supplementary Table 5 | SO features: Data are means ± s.e.m. Duration and relative occurrence during N2 and N3 sleep for scalp (ANT and MD analyses related), ANT and MD derived SOs.

SO	Duration [sec]	Rel. N2 [%]	Rel. N3 [%]
scalp $_{ANT}$	1.31 ± 0.01	46.56 ± 3.79	53.43 ± 3.79
scalp $_{MD}$	1.31 ± 0.02	47.41 ± 4.38	52.58 ± 4.38
ANT	1.30 ± 0.01	46.05 ± 3.68	53.94 ± 3.68
MD	1.31 ± 0.02	47.18 ± 4.93	52.81 ± 4.93

Supplementary Table 6 | spindle features: Data are means ± s.e.m. Peak frequency, duration and relative occurrence during N2 and N3 sleep for scalp (ANT and MD analyses related), ANT and MD derived spindles

spindles	Peak-Freq [Hz]	Duration [ms]	Rel. N2 [%]	Rel. N3 [%]
scalp $_{ANT}$	13.02 ± 0.15	0.81 ± 0.03	73.71 ± 3.81	26.29 ± 3.81
scalp $_{MD}$	13.07 ± 0.13	0.77 ± 0.05	70.68 ± 5.14	29.32 ± 5.14
ANT	13.17 ± 0.09	0.79 ± 0.04	73.51 ± 3.76	26.49 ± 3.76
MD	13.03 ± 0.11	0.78 ± 0.03	74.02 ± 3.49	25.97 ± 3.49

Supplementary Table 7 | drug regimen at the time of recordings.

	Anticonvulsant
P1	Levetiracetam, Phenytoin, Lamotrigine
P2	Levetiracetam, Lamotrigine
P3	Lacosamide, Oxcarbazepine, Topiramate
P4	Levetiracetam, Lamotrigine, Oxcarbazepin, Zonisamide
P5	Levetiracetam, Lamotrigine
P6	Lamotrigine, Lacosamide, Zonisamide
P7	Oxcarbazepin, Topiramate
P8	Topiramate

Supplementary Table 8 | Documented effects drugs on sleep architecture.

Drug	Effect on sleep
Lacosamide[1]	none
Lamotrigine[2]	REM↑, N2↑, SWS↓
Levetiracetam[3]	N2↑, REM↓
Oxcarbazepine	unknown
Phenytoin[4]	SWS↓, REM↓
Topiramate[5]	none
Zonisamide[6]	none

1) Hudson J.D., Guptil J.T., Bynes W., et al. (2015). Assessment of the effects of lacosamide on sleep parameters in healthy subjects. Seizure; 25: 155-159 2) Placidi F, Marciani MG, Diomedi M, et al (2000). Effects of lamotrigine on nocturnal sleep, daytime somnolence and cognitive functions in focal epilepsy. Acta Neurol Scand;102:81–86. 3) Cicolin A, Magliola U, Giordano A, et al. (2006). Effects of levetiracetam on nocturnal sleep and daytime vigilance in healthy volunteers. Epilepsia; 47:82–85. 4) Benjamin Legros & Carl W Bazil (2003). Effects of antiepileptic drugs on sleep architecture: a pilot study. Sleep Med; 4(1):51-5. 5) Bonanni E, Galli R, Maestri M, et al. (2004). Daytime sleepiness in epilepsy patients receiving topiramate monotherapy. Epilepsia; 45:333–337. 6) Romigi A, Izzi F, Placidi F, et al (2013). Effects of zonisamide as add-on therapy on sleep-wake cycle in focal epilepsy: a polysomnographic study. Epilepsy Behav; 26:170–174.

Supplementary figures

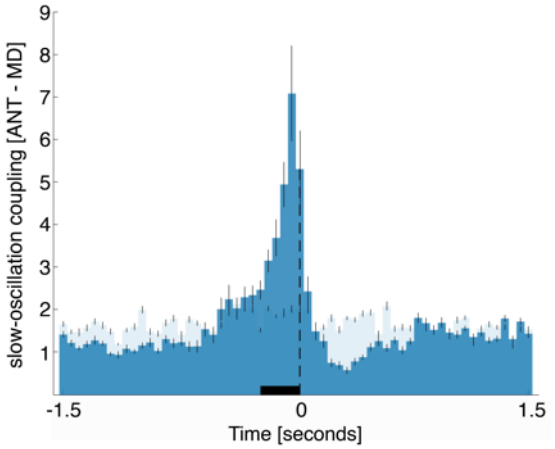

Supplementary Fig. 1 | SO coupling ANT-MD: Occurrence probabilities of ANT SO down state peaks relative to MD SO down state peaks (time = 0; dashed line), indicating that ANT SOs precede on average MD SOs, when directly compared (i.e., without taking neocortical coordination into account, as in Fig. 2 The solid black line indicates significant time bins, resulting from comparison with SO-free control events (significant positive cluster from -0.25 to 0 sec, p = 0.041; time of peak: -0.05 sec).

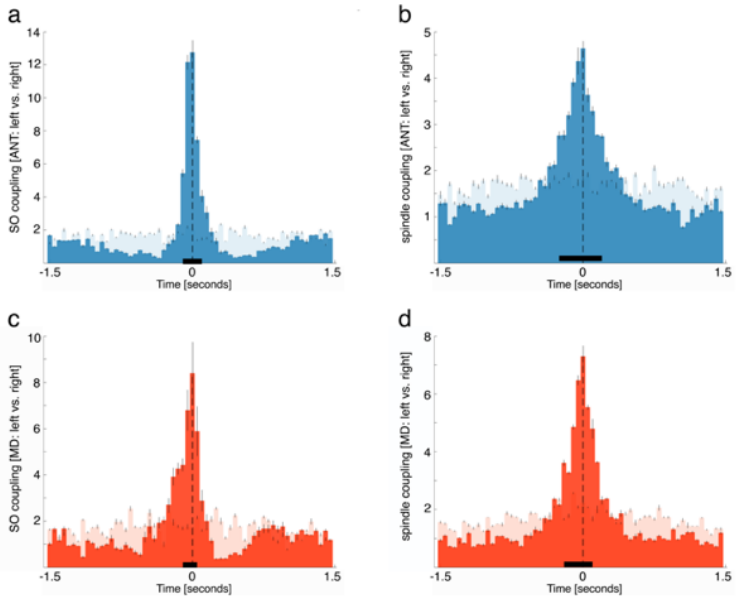

Supplementary Fig. 2 | Lateralization of coupling: (a) Occurrence probabilities of left ANT SO down state peaks relative to right ANT SO down state peaks, indicated that SOs in the left and right ANT emerged synchronously (significant positive cluster from -0.1 to 0.1 sec; p < 0.0001; time of peak = 0 sec). **(b)** Occurrence probabilities for sleep spindles derived from the left ANT, relative to right ANT detected spindles, indicated that SOs in the left and right ANT emerged synchronously (significant positive cluster from -0.25 to 0.25 sec; p < 0.0001; time of peak = 0 sec). **(c)** Occurrence probabilities of left MD SO down state peaks relative to right MD SO down state peaks, (significant positive cluster from -0.15 to 0.05 sec; p < 0.0001; time of peak = 0 sec). **(d)** Occurrence probabilities for sleep spindles derived from the left MD, relative to right MD detected spindles (significant positive cluster from -0.2 to 0.1 sec; p < 0.0001; time of peak = 0 sec).

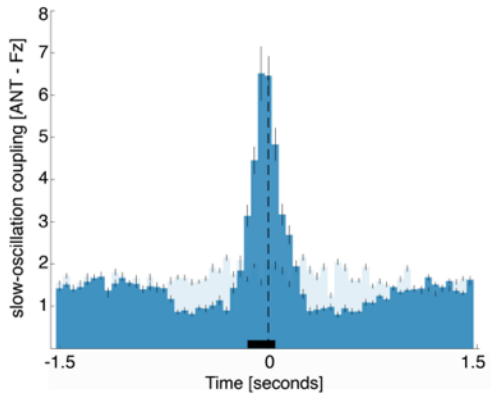

Supplementary Fig. 3 | SO coupling ANT-Fz: Occurrence probabilities of ANT SO down state peaks relative to SO down state peaks derived from scalp electrode Fz (time = 0; dashed line), supporting the main finding that ANT SOs precede neocortical SOs. The solid black line indicates significant time bins, resulting from comparison with SO-free control events (significant positive cluster from -0.15 to 0.05 sec, $p < 0.005$; time of peak: -0.05 sec). Note that Fz was not used as generic seed electrode in the main analysis (Fig. 1a), as it was contaminated with epileptic activity in 3/8 patients.

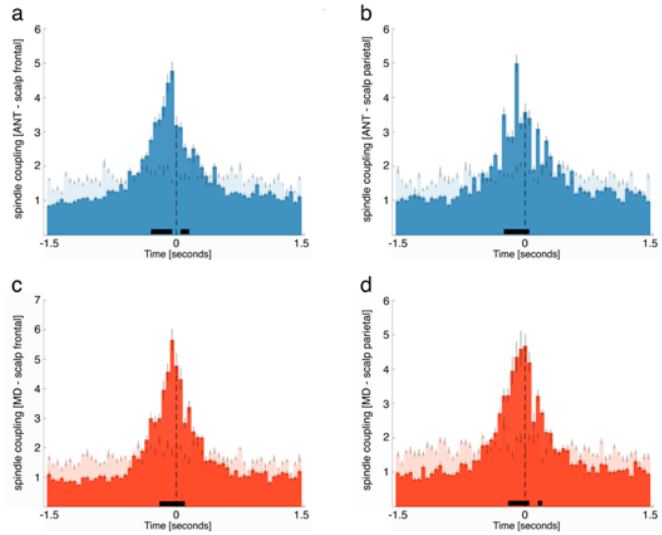

Supplementary Fig. 4 | Thalamic spindles coupled to frontal and parietal scalp spindles: (a + b) Occurrence probabilities of ANT spindle peaks relative to frontal **(a)** and parietal **(b)** neocortical spindle peaks (maximal negative amplitude, time = 0), indicating that ANT spindles precede neocortical spindles detected from both frontal and parietal scalp electrodes (frontal: first significant positive cluster from -0.3 to -0.05 sec, $p < 0.001$; second cluster from 0.05 to 0.15 sec, $p = 0.005$; time of peak: -0.05 sec; parietal: significant positive cluster from -0.25 to 0.05 s, $p < 0.001$). **(c + d)** Occurrence probabilities of MD spindle peaks relative to frontal **(c)** and parietal **(d)** neocortical spindle peaks (maximal negative amplitude, time = 0), indicating that MD spindles precede neocortical spindles detected from both frontal and parietal scalp electrodes (frontal: significant positive cluster from -0.2 to 0.1 sec, $p < 0.001$; time of peak: -0.05 sec; parietal: first significant positive cluster from -0.2 to 0.05 sec, $p < 0.001$; second significant positive cluster from 0.15 to 0.2 sec, $p = 0.01$; time of peak = 0).